Pure Appl. Chem., Vol. 83, No. 9, pp. 1763–1779, 2011.
doi:10.1351/PAC-CON-10-11-22

Desired properties of new phthalocyanines for photodynamic therapy*

Tebello Nyokong

Department of Chemistry, Rhodes University, Grahamstown, South Africa

Abstract: The manuscript focuses on the properties of phthalocyanines (Pcs) that are required for them to be employed as photosensitizers in applications such as photodynamic therapy (PDT). High triplet-state quantum yields and lifetimes as well as high singlet-oxygen quantum yields are required for a good photosensitizer. In addition, absorption of the photosensitizer in the red region of the electromagnetic spectrum is also required, and this can be achieved by ring expansion, substitution with electron-donating ligands, and change of the central metal among others. Quantum dots (QDs) are efficient accumulators of light energy, and they can transfer this energy to molecules that possess a very efficient ability to generate singlet oxygen through a process called Förster resonance energy transfer (FRET). Thus, there is a decrease in the fluorescence quantum yield of the QDs when in the vicinity of Pcs. Triplet quantum yields of the Pcs increase in the presence of QDs.

Keywords: energy transfer; phthalocyanines; photochemistry; photophysics; quantum dots.

INTRODUCTION

Phthalocyanines (Pcs, Fig. 1a) and metallophthalocyanines (MPcs) have a wide variety of applications due to their diverse chemical, structural, electronic, and optical properties. Pcs continually find their usefulness in contemporary and emerging technologies such as catalysis, photodynamic therapy (PDT), nonlinear optics, gas sensors, thermal writing displays, and solar cells [1–7]. Specificity in the applications of Pcs can be introduced by modification of the Pc ring or by changes in the central metal or axial ligands. The PDT modality combines a light-sensitive drug with the selectivity of fiber-optic-directed light and the cell destruction properties of singlet oxygen (or other radicals). Requirements for a good photosensitizer include: (i) absorption in the near-infrared (NIR) region, (ii) high triplet-state quantum yields and lifetimes as well as high singlet-oxygen quantum yields, (iii) high specificity for the target tissue, and (iv) water solubility. In this review, we discuss the design of Pcs that will enhance these properties.

Since the survival and quality of life of cancer patients is also linked to an optimal and reliable diagnosis, there is a need for new imaging techniques that are sensitive and disease-specific. The combination of MPcs with quantum dots (QDs) may allow for an efficient cancer treatment involving photosensitization (PDT) and imaging using QDs. QDs are also photosensitizers for PDT, hence their combination with Pcs may improve PDT activity of the latter.

*Paper based on a presentation made at the 11th Eurasia Conference on Chemical Sciences, The Dead Sea, Jordan, 6–10 October 2010. Other presentations are published in this issue, pp. 1643–1799.

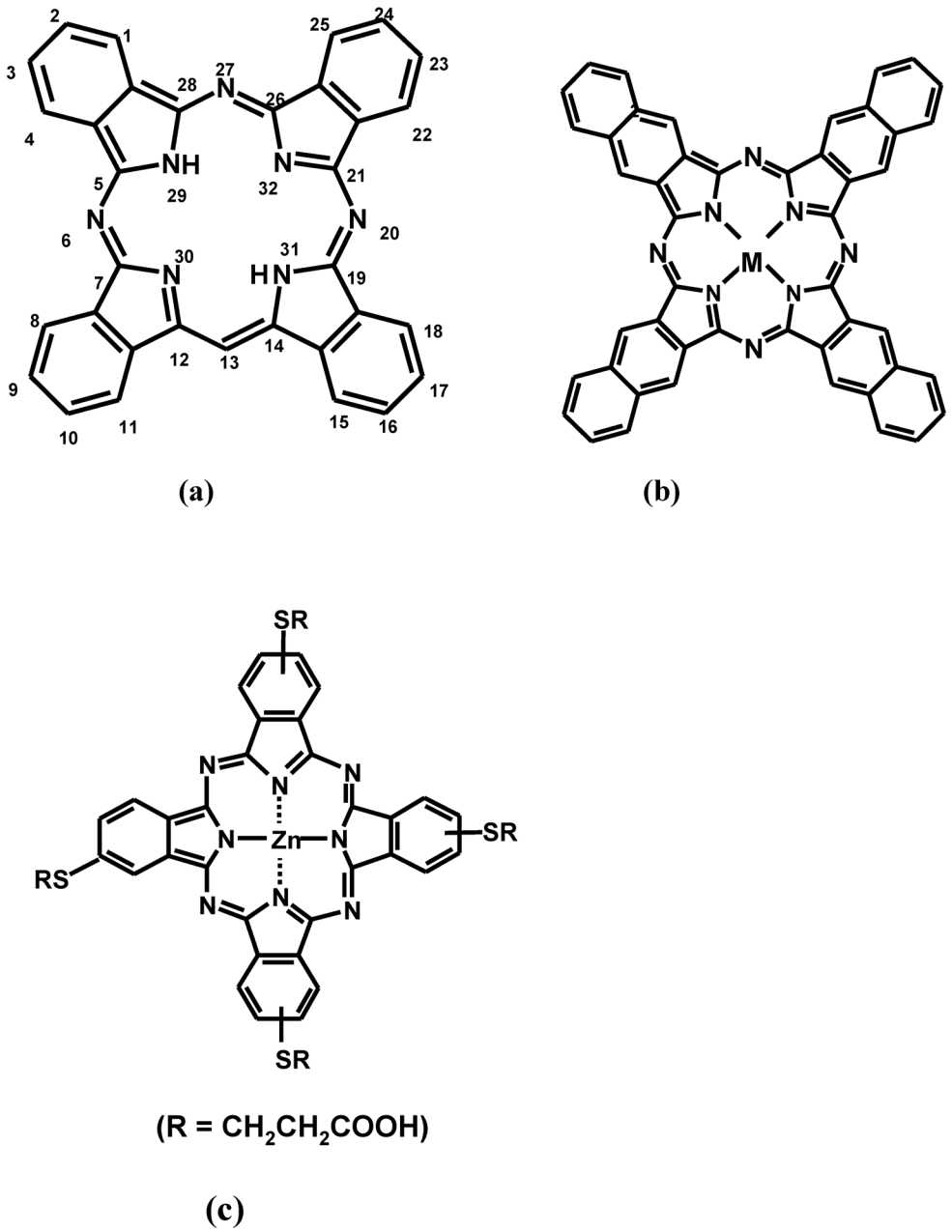

Fig. 1 Molecular structures of (a) metal-free Pc, (b) MPc, and (c) water-soluble mercaptopropanoic acid tetra-substituted (ZnMTPc).

NEAR-INFRARED (NIR) ABSORBING PHTHALOCYANINE COMPLEXES

Since there is minimal light scattering and absorption in the NIR region of the spectrum, light of low intensity can be used to penetrate into tissue to depths of several centimeters, thereby allowing access to deep-seated tumors. Hence, Pcs that absorb in the NIR region are essential for PDT applications. The spectra of Pcs are governed by 18 π-system of the inner 16-membered ring. The spectra consist of intense absorption band in the visible region near 670 nm called the Q-band and a generally weak band

near 340 nm called the Soret or B-band. Charge-transfer bands between the central metal and the ring are also observed for some Pc complexes. The color of the Pc molecules is in general determined by the Q-band. But for highly red-shifted MPc complexes, the Q-band no longer determines the color.

Extension of π-conjugation

It is well established that expansion of the π-conjugation in Pcs shifts the Q-band to the red [8]. Extension of the conjugation system is accompanied by change in color from blue/green to colors including brown, red, or purple. Naphthalocyanines (Ncs, Fig. 1b) are shifted to the red in comparison with the corresponding Pcs. The same applies to benzohelicenocyanine (BHc) and helicenocyanine (Hc) [9]. However, the stabilities of Nc, Hc, and BHc molecules are low, compared to Pcs in general. Kobayashi and co-workers have performed extensive calculations on the molecular orbitals of the Pcs and related molecules and have shown that red-shifting resulting from ring expansion is due to destabilization of the highest occupied molecular orbital (HOMO) [8]. Destabilization of the HOMO increases with addition of benzene units to the Pc ring in a linear fashion [8].

Electron-donating substituents

Addition of electron-donating groups on the Pc ring results in a red-shift of the Q-band of Pcs to the NIR region. Substitution of the ring with sulfur-containing groups results in a large red-shift of the Q-band, due to the electron-donating ability of these groups, Fig. 2 [10]. Amino-substituted MPc complexes are also red-shifted compared to unsubstituted complexes, due to the electron-donating nature of the amino group [9].

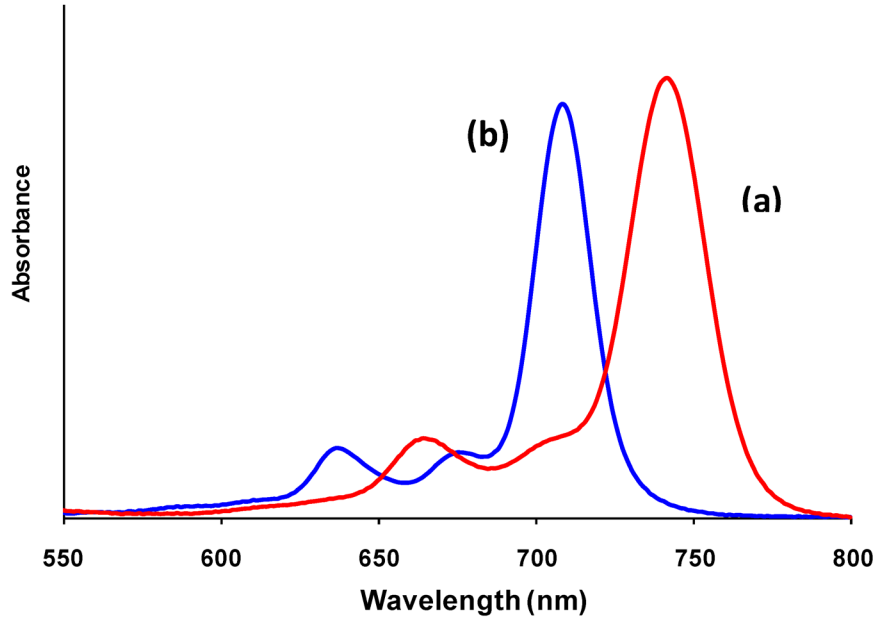

Fig. 2 Electronic absorption spectra of tetra-substituted phenylthio (a) and oxophenoxy (b) (phthalocyaninato)titanium(IV) in DMSO. Concentration ~1.4×10^{-5} M. Adapted from ref. [10].

Change in central metal

Another method of obtaining red-shifted MPc spectra is by choice of the central metal. The effect of the central metal in MPc complexes is usually small except for a few metals such as Mn, Sb, Bi, V, and Sn. Considering the same substituents $\{(SC_5H_{11})_8\}$, there is a red-shift in the Q-band on going from Ti^{IV} (808 nm) [11] to V^{IV} (850 nm) [12] and Mn^{III} (893 nm) [11]. However in terms of applications to PDT, some of these metals are not ideal due to their paramagnetic nature. A large red-shift has been attributed to highly deformed Pc skeleton due to the central metals not fitting into the cavity of the Pc molecule. The deformed Pc ligand then interacts with the protruding central metal, hence the observed red-shifting of the spectra [13].

Point of substitution

In general, the effects of non-peripheral substitution (at 1,4-position; see Fig. 1 for numbering) of a Pc on its Q-band position are larger than observed for peripheral substitution (2,3-position). Particularly, substituents that allow themselves to conjugate with the 18 π-system at the 1,4-position cause a large red-shift of the Q-band as compared to substituents at the 2,3-position [9,14]. Good examples are peripherally substituted manganese tetra amino phthalocyanine $\{\beta\text{-}Mn^{III}Pc(NH_2)_4\}$, which absorbs at 780 nm [15], while non-peripherally substituted derivative absorbs at 871 nm [16]. Non-peripherally substituted $TiPc(NH_2)_4$ shows a Q-band at 830 nm [17] compared to 755 nm observed for peripherally substituted derivative. A large shift to NIR region was reported for MPcs containing alkyl thio substituents at non-peripheral positions, with increase in the number of these substituents, from $(Cl)_2SnPc(C_{12}H_{25})_4$ to $(Cl)_2SnPc(C_{12}H_{25})_8$ [9].

WATER-SOLUBLE PHTHALOCYANINES

Amphiphilic Pcs have been considered as candidates for PDT [3] since the drug will have to be injected into the blood stream and traverse lipid membranes. Thus, synthesis of water-soluble Pc molecules is of utmost importance. A recent review describes methods of synthesizing water-soluble Pc complexes [18]. Anionic substituents which confer water solubility to Pcs include sulfonate, carboxylate, and phosphorus-based functionalities, attached directly on the macrocycle or borne by various spacers. Cationic Pcs are also water-soluble. Water solubility for cationic Pcs is achieved by the quaternization of aliphatic or aromatic nitrogen atom on the formed Pc. Several types of non-ionic substituents are also able to confer water solubility to Pcs. These include: polyethylene-glycol, carbohydrate, and other polyhydroxylated groups [18].

Water-soluble Pcs tend to be aggregated, which is the limitation in terms of their application as photosensitizers. Aggregates of monomers (such as in tetrasulfonated Pcs) in water are not chemically bonded but exist as loosely associated species which can be dissociated by an organic solvent. For aggregated systems, it is expected that dilution will change the Q-band shape. In most cases, aggregation due to the cofacial conformation (the so-called H aggregates) between the chromophores gives rise to a blue-shift of the Q-band. In contrast, red-shifts of the Q-band are due to a slipped-cofacial alignment of the Pc rings (the so-called J aggregates) which is a much less common form of aggregation in solution chemistry of Pcs. Aggregation reduces the lifetimes of the MPc excited state, most probably due to enhanced radiationless excited-state dissipation. Quantum yields of the excited states, and consequently singlet-oxygen generation, are lowered for aggregated species. For sulfonated complexes, the degree of sulfonation, isomeric composition, and the nature of the central metal ion affect the extent of aggregation. Biological environments support monomerization of Pcs.

SELECTIVITY

Recently, several new strategies aimed at improving the performances of PDT agents have emerged. These include carrier proteins, carbohydrates, or hydrophilic polymers for selective delivery of the agents into tumor tissues. The vitamin B9 (also called folic acid), for example, is a ligand able to target covalently attached bioactive agents quite specifically to folate receptor (FR)-positive cancer cells. FRs are overexpressed by many types of tumor cells, including ovarian, endometrial, colorectal, breast, lung, renal, neuroendocrine carcinomas, and brain metastases. Proper synthesis procedures have been developed to link folic acid to molecules such as porphyrins in order to develop targeting delivery systems [19], and high levels of selectivity to tumor cells have been reported. Attaching Pcs to biological molecules such as estrone and cholesterol has been reported as a way of introducing selectivity [20].

PHOTOPHYSICAL AND PHOTOCHEMICAL BEHAVIOR

It is believed that during photosensitization in PDT, the MPc molecule is first excited to the triplet state, and then transfers the energy to ground-state oxygen, $O_2(^3\Sigma_g)$, generating excited-state oxygen, $O_2(^1\Delta_g)$, the chief cytotoxic species, which subsequently oxidizes the substrate. This is the type II mechanism as shown in Scheme 1 [21–23], eqs. 1–3.

$$MPc \rightarrow {}^1MPc^* \xrightarrow{ISC} {}^3MPc^* \quad (1)$$

$${}^3MPc^* + {}^3O_2 \rightarrow {}^1O_2 \quad (2)$$

$${}^1O_2 + subs \rightarrow \text{oxidation products} \quad (3)$$

Scheme 1 Type II mechanism. MPc is the metallophthalocyanine, ISC is intersystem crossing and subs is the substrate. $^3O_2$ represents $O_2(^3\Sigma_g)$ and $^1O_2$ represents $O_2(^1\Delta_g)$.

Another mechanism (type I) may also be involved in photosensitization. In type I mechanism, the excited triplet state of the MPc (^{3}MPc*) interacts with ground-state molecular oxygen or substrate molecules generating superoxide (eqs. 4 and 6) and hydroperoxyl radicals (eq. 7), which subsequently afford oxidation of the substrate (eqs. 8 and 9), Scheme 2 [21].

$${}^3MPc^* + O_2 \rightarrow MPc^{+\bullet} + O_2^{-\bullet} \quad (4)$$

$${}^3MPc^* + subs \rightarrow MPc^{-\bullet} + subs^{+\bullet} \quad (5)$$

$$MPc^{-\bullet} + O_2 \rightarrow MPc + O_2^{-\bullet} \quad (6)$$

$$O_2^{-\bullet} \rightarrow HO_2^{\bullet} \quad (7)$$

$$HO_2^{\bullet} + \text{subs-H} \rightarrow H_2O_2 + subs^{\bullet} \quad (8)$$

$$subs^{+\bullet}, subs^{\bullet}, H_2O_2 \rightarrow \text{oxidation products} \quad (9)$$

Scheme 2 Type I mechanism. MPc = metallophthalocyanine, subs = substrate.

It has been reported that the type II mechanism is the most prevalent in photosensitized reactions. Hence, singlet-oxygen quantum yield is an important parameter. High triplet-state quantum yields are necessary in order to produce high singlet-oxygen quantum yields. Thus, triplet- and singlet-oxygen quantum yields as well as triplet-state lifetimes are essential for the study of molecules aimed for application in PDT.

Triplet-state quantum yields and lifetimes

Laser flash photolysis gives information about the triplet–triplet absorption and the lifetime of the excited species. The triplet quantum yield (Φ_T) calculations are generally based on the maximum absorption of the triplet state generated during laser flash photolysis experiments. The triplet-state absorption of MPcs is in the range 400–600 nm, a region which is far away from their ground-state absorption maximum (Q-band ~700 nm), Fig. 3 (inset a). This provides an easy measurement of the triplet absorption since there is no overlap. The transient absorption due to the triplet state between 400 and 600 nm is accompanied by loss in the absorption in the Soret and Q-band regions due to depletion of the parent compounds, Fig. 3. The decay curve in Fig. 3 (inset b) is employed in the calculation of triplet quantum yields. In general, a relative method using the triplet absorption [23,24] is employed for triplet quantum yield calculations, eq. 10.

$$\Phi_T = \Phi_T^{std} \frac{\Delta A_T A_T^{std}}{\Delta A_T^{std} \varepsilon_T} \tag{10}$$

where ΔA_T and ΔA_T^{std} are the changes in the triplet-state absorption of the MPc derivative and the standard, respectively. Φ_T^{std} (= 0.65 for, e.g., ZnPc standard in dimethylsulfoxide, DMSO [24]) is the triplet-state quantum yield for the standard. ε_T and ε_T^{std} are the triplet-state extinction coefficients for the MPc derivatives and the standard, respectively, and are determined from the molar extinction coefficients of their respective singlet states (ε_s and ε_s^{std}), the changes in absorbances of the ground singlet states (ΔA_S and ΔA_S^{std}) and changes in the triplet-state absorptions, (ΔA_T and ΔA_T^{std}) according to eqs. 11 and 12.

$$\varepsilon_T = \varepsilon_S \frac{\Delta A_T}{\Delta A_S} \tag{11}$$

$$\varepsilon_T^{std} = \varepsilon_S^{std} \frac{\Delta A_T^{std}}{\Delta A_S^{std}} \tag{12}$$

A decay curve (Fig. 3, inset b) also gives the triplet lifetime. The lifetimes of the transients are determined from a software program such as OriginPro 7.5, used in fitting the triplet decay curve. Table 1 lists triplet quantum yields of sulfonated Pc complexes containing a mixture of differently sub-

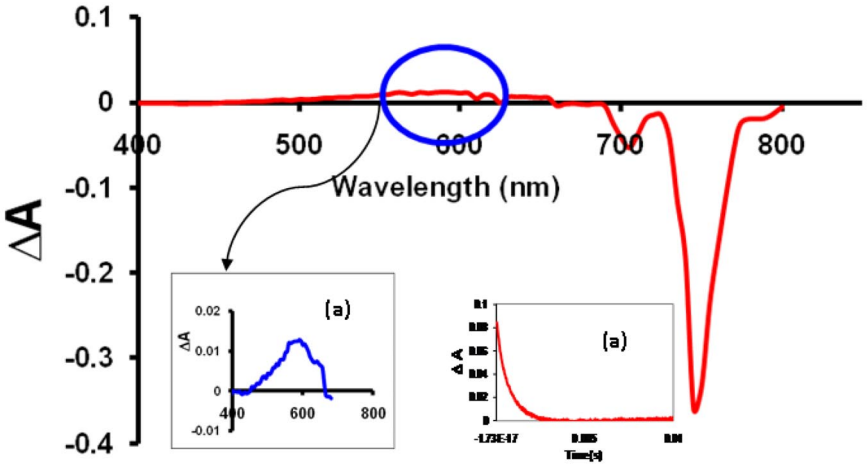

Fig. 3 Typical differential absorption spectrum of an MPc. Inset (a): expansion of the triplet–triplet absorption. Inset (b): typical triplet decay curve of MPc. Adapted from ref. [43].

stituted derivatives ($MPcS_{mix}$ in water [25]). There is a clear dependence of the Φ_T values on the size of the central metal. The values increase with size due to the heavy atom effect, where Sn central atom gives the largest value of Φ_T. The triplet lifetimes are smaller for the larger central atoms such as tin and larger for Al as a central metal. The heavy atom effect is the enhancement of the rate of a spin-forbidden process by the presence of an atom of high atomic number, which is either part of, or external to, the excited molecular entity. Mechanistically, it responds to a spin-orbit coupling enhancement produced by a heavy atom.

Table 1 Triplet-state quantum yields and lifetimes, and singlet-oxygen quantum yields for $MPcS_{mix}$ in water [25].

Complex	τ_T (μs)	Φ_T	Φ_Δ
$AlPcS_{mix}$	800	0.52	0.48
$SiPcS_{mix}$	430	0.58	0.52
$GePcS_{mix}$	760	0.79	0.78
$SnPcS_{mix}$	120	0.87	0.65
$ZnPcS_{mix}$	530	0.86	0.72

Singlet-oxygen quantum yields (Φ_Δ)

The singlet-oxygen quantum yields for the MPc complexes may be conveniently determined using a singlet-oxygen quencher such as 1,3-diphenylisobenzofuran (DPBF) in organic solvents or by using the singlet-oxygen luminescence method (SOLM) [26]. DPBF is an efficient $^1O_2$ quencher in organic solvents, and its disappearance can be readily monitored by following the decrease in its absorption peak at 416 nm (e.g., in DMSO), Fig. 4. Anthracene-9, 10-bis-methylmalonate (ADMA), may be employed as a singlet oxygen quencher in aqueous media by monitoring its disappearance at 380 nm in the presence of singlet oxygen [27].

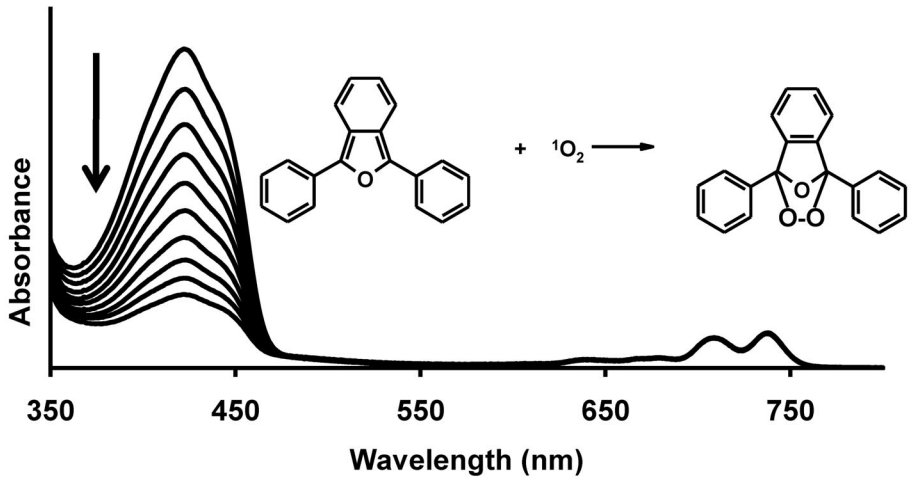

Fig. 4 Change in absorption spectra of DPBF as singlet oxygen is produced by the Pc. Inset = representation of the reaction of singlet oxygen with DPBF.

A relative method (using eq. 13) may be employed for singlet-oxygen calculations [28,29].

$$\Phi_{\Delta} = \Phi_{\Delta}^{std} \frac{W \cdot I_{abs}^{std}}{W^{std} \cdot I_{abs}} \tag{13}$$

where Φ_{Δ}^{std} is the singlet-oxygen quantum yield for the standard, W and W^{std} are the DPBF photobleaching rates in the presence of MPc derivatives under investigation and the standard, respectively. I_{abs} and I_{abs}^{std} are the rates of light absorption by the MPc derivative and standard, respectively. ZnPc is often used as a standard (e.g., Φ_{Δ}^{std} = 0.67 in DMSO) [30,31].

The use of the SOLM relies on the luminescence of singlet oxygen at 1270 nm, which is a spin-forbidden process ($S_1 - T_1$), but occurs in an area that is generally free from interference. A typical signal is shown in Fig. 5. The dynamic course of $^1O_2$ concentration [$^1O_2$] can be clearly recorded, following eq. 14 as described theoretically in the literature [32].

$$I = A \frac{\tau_D}{\tau_T - \tau_D} [\exp(\frac{-t}{\tau_T}) - \exp(\frac{-t}{\tau_D})] \tag{14}$$

where τ_D is the lifetime of $^1O_2$, τ_T is the lifetime of MPc at the triplet state, t is time in seconds, I is the luminescence intensity, and A is a coefficient involved in sensitizer concentration and singlet-oxygen quantum yield. The singlet-oxygen quantum yield may then be determined by the relative method using a standard such as ZnPc (eq. 15).

$$\Phi_{\Delta} = \Phi_{\Delta}^{std} \frac{A}{A^{std}} \tag{15}$$

where Φ_{Δ}^{std} is the singlet-oxygen quantum yield for the standard, A and A^{std} are the coefficients of the sample and standard, respectively. Table 1 shows examples of singlet quantum yields of sulfonated Pc complexes containing a mixture of differently substituted derivatives ($MPcS_{mix}$ in water [25]). There is a dependence of the Φ_{Δ} values on the size of the central metal. The values increase with size, where the smaller central metal Al, gives a smaller Φ_{Δ} value, and Zn gives a larger value. The Φ_{Δ} value obtained when Sn is the central metal does not correspond to the large triplet quantum yield for the complex, suggesting inefficient energy transfer (ET).

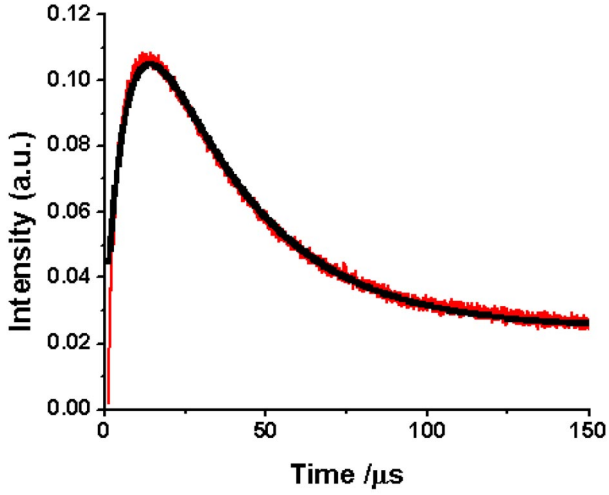

Fig. 5 Typical decay curve observed during singlet-oxygen determination using its luminescence at 1270 nm.

INTERACTION OF PHTHALOCYANINES AND QUANTUM DOTS

When two or more substances are used for curing one disease, the term "combination therapy" is often employed. This is useful when the combined complexes have better therapeutic properties than their components taken separately. Recently, QDs have found focus as a new generation of photosensitizers in PDT [33–36]. QDs are capable of transferring energy to ground-state molecular oxygen to generate cytotoxic singlet oxygen and thus enhance the efficacy of PDT [35,37,38]. The singlet-oxygen-generating capabilities of QDs are, however, very limited [33], therefore, conjugation of QDs to a mediating PDT photosensitizer (e.g., an MPc) facilitates the probability of increased PDT efficiency through ET.

QDs are defined as 0-dimensional semiconductor materials as a result of quantum confinement of electrons in all three physical dimensions. Of particular interest is their broad absorption spectrum, which allows excitation over a broad range of wavelengths and their size tunable narrow emission spanning the ultraviolet (UV) to infrared region [39], Fig. 6, which makes them well suited for imaging applications [40,41]. QDs are efficient accumulators of the incident light energy with extremely low inner losses, and they can transfer this energy to molecules that possess very efficient ability to generate singlet oxygen through a process called Förster resonance energy transfer (FRET).

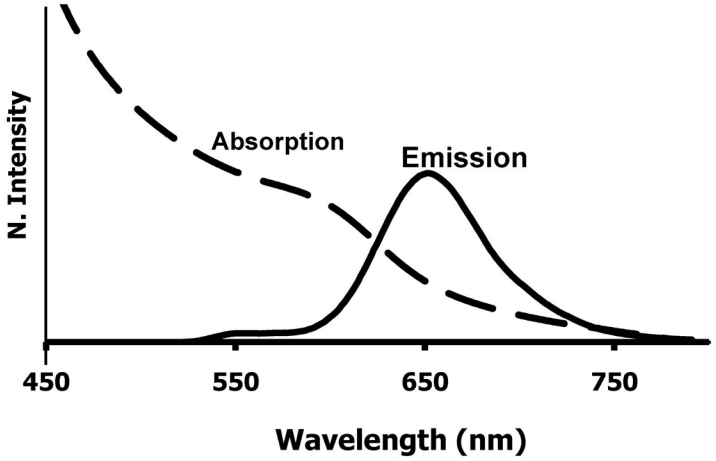

Fig. 6 Absorbance and emission spectra of MPA-capped CdTe QDs (1 mg/1 mL, in (1:1) ethanol: 0.01 M NaOH solvent mixture, $\lambda_{excitation}$ = 500 nm).

Water-soluble quantum dots

QDs which are not soluble in aqueous media are not useful for application in biomedical applications. Water-soluble, thiol-stabilized QDs are being synthesized routinely [42–44], using different types of thiols. The thiols usually employed include thioglycolic acid (TGA), mercaptopropionic acid (MPA) and L-cysteine (L-Cys). The nature of the thiol influences the photoluminscence of QDs.

The growth of QDs, during their synthesis, can be explained by the Ostwald ripening process, i.e., during growth, smaller particles dissolve and become the constituents of larger particles. A shift in emission wavelength to the red with increase in particle size is a well-known phenomena.

X-ray powder diffraction (XRD) is often used for QDs size determination, Fig. 7, using the Scherrer eq. 16.

$$d = \frac{k\lambda}{\beta \cos\theta} \tag{16}$$

where k corresponds to an empirical constant (0.9), λ is the X-ray source wavelength (1.5405 Å), β is the full width at half maximum of the diffraction peak, and θ is the angle of the peak. The sizes of water-soluble CdTe QDs capped with TGA, MPA, or L-Cys range between 3 to 5 nm.

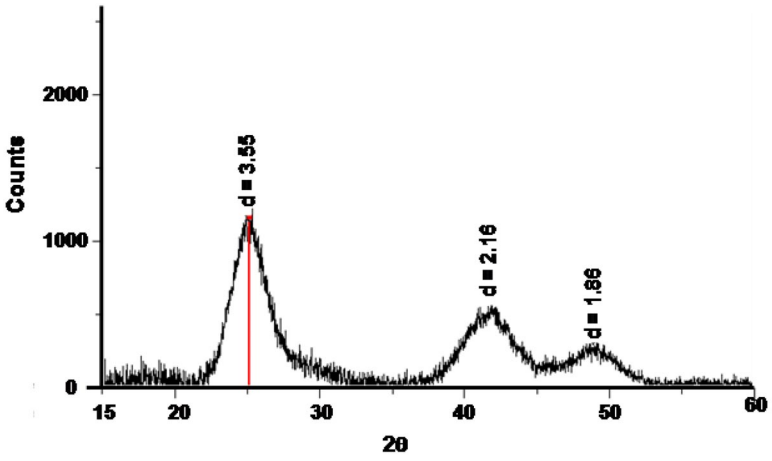

Fig. 7 XRD plot for CdTe-MPA-capped QDs.

The carboxylic acid groups that terminate the thiol-capped CdTe QDs may be linked to the amino groups attached to the Pc ring, through an amide bond, Scheme 3. Coupling agents such as dicyclohexylcarbodiimide (DCC), *N*-ethyl-*N*-(3-dimethylaminopropyl) carbodiimide (EDC), and *N*-hydroxy succinimide (NHS) may be employed to facilitate formation of an amide bond.

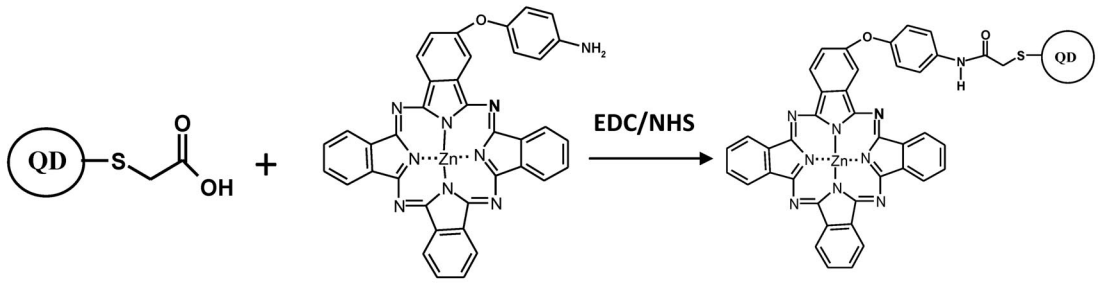

Scheme 3 The formation of an amide bond between zinc mono(4-aminophenoxy) phthalocyanine (ZnMAPPc) and CdTe QDs. EDC = *N*-ethyl-N(3-dimethylaminopropyl) carbodiimide, NHS = *N*-hydroxy succinimide.

Fluorescence quantum yields

Fluorescence quantum yields ($\Phi_{F(QDs)}$) of QDs may calculated using eq. 17 [45]

$$\Phi_F = \Phi_{F(std)} \frac{F.A_{std}.n^2}{F_{std}.A.n_{std}^2} \tag{17}$$

where F and F_{std} refer to the integrated fluorescence intensity of the MPc and the reference, respectively. A and A_{std} are the absorbances of the sample and reference at the excitation wavelength, respectively, and n and n_{std} are the refractive indices of solvents used for the sample and reference, respec-

tively. Rhodamine 6G in ethanol ($\Phi_F = 0.95$ [46]) may be employed as a standard for the determination of the fluorescence quantum yields of the quantum dots ($\Phi_{F(QD)}$). Both the sample and reference are excited at the same wavelength.

The quantum yield values determined for the QDs are then employed in the determination of their fluorescence quantum yields in the mixture ($\Phi^{mix}_{F(QD)}$) or linked ($\Phi^{linked}_{F(QD)}$) with Pcs, using eqs. 18 and 19

$$\Phi^{mix}_{F(QD)} = \Phi_{F(QD)} \frac{F^{mix}_{QD}}{F_{QD}} \tag{18}$$

$$\Phi^{linked}_{F(QD)} = \Phi_{F(QD)} \frac{F^{linked}_{QD}}{F_{QD}} \tag{19}$$

where $\Phi_{F(QD)}$ represents the fluorescence quantum yield of the QDs alone, and is used as a standard, $F^{mix}_{F(QD)}$ or $F^{linked}_{F(QD)}$ are the fluorescence intensities of QDs in the mixture with Pcs or linked to them, respectively. The excitation must be at the wavelength where QDs absorb and Pcs do not. F_{QD} is the fluorescence intensity of the QDs alone.

In general, the fluorescence quantum yields of QDs in the mixture with (or linked to) Pcs are reduced relative to Φ_F values of the QDs alone, due to quenching as a result of transfer of energy from donor QDs to Pc acceptor molecules [44,47], Table 2. This results in a lowering of QD fluorescence intensity. Nonradiative (NR) decay processes may also be used to account for the decline in Φ_F values. Table 2 shows that there a larger decrease in Φ_F values for the linked complex. Thus, in the presence of MPc complexes and on excitation at the wavelength where QDs absorb, there is a large decrease in the Φ_F values of the QDs due to ET discussed below.

Table 2 The fluorescence behavior of QDs in the absence and presence of ZnMAPPc (see Scheme 3 for molecular structure). DMSO:water (9:1) [47].

Thiol capping	$\Phi_{F(QD)}$	$\Phi^{mix}_{F(QD)}$	$\Phi^{linked}_{F(QD)}$
MPA (3.9)	0.57	0.21	0.04
TGA (3.4)	0.57	0.48	0.03
LCys (4.1)	0.04	0.03	0.004

Fluorescence lifetimes

Fluorescence lifetimes of the QDs are obtained by deconvolution of the decay curves, obtained from time-correlated single photon counting (TCSPC), an example of a TCSPC curve is shown in Fig. 8.

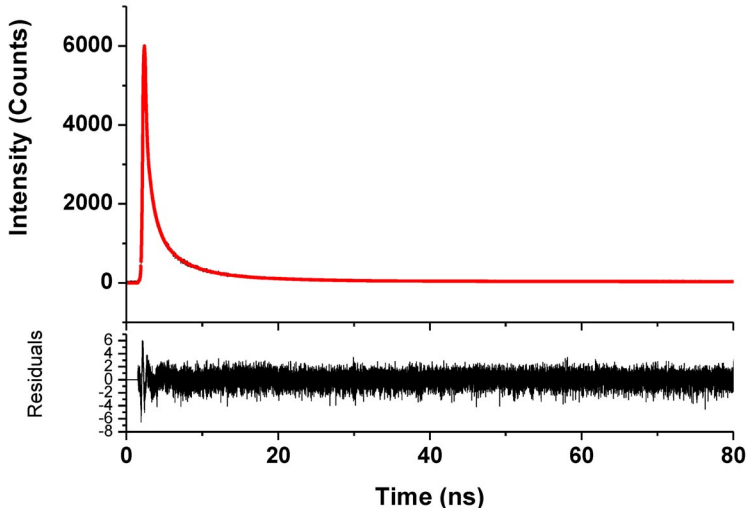

Fig. 8 Fluorescence decay curves of CdTe QDs (MPA-capped) in the presence of the molecule (ZnMAPPc) shown in Scheme 3.

The fluorescence lifetimes are listed in Table 3 for QDs alone or in the presence of MPc complexes. The presence of three lifetimes is common occurrence for QDs. Though there is lack of agreement in literature, the longer lifetime (τ_1 in Table 3) component is usually associated with the involvement of surface states in the carrier recombination process [48]. The intermediate lifetime (τ_2 in Table 3) component may be attributed to the intrinsic recombination of initially populated core states [49–51] and the shortest lifetime (τ_3 in Table 3) is attributed to radiative depopulation due to band edge recombination at the surface. Table 3 shows that MPA-capped QDs gave the largest decrease (~26 %) in the longest lifetime (τ_1) in the presence of ZnMAPPc (see Scheme 3 for the structure), compared to the other two QDs.

Table 3 Fluorescence lifetimes of MPA, L-cys, and TGA-capped QDs in the absence or mixed with ZnMAPPc (see Scheme 3 for molecular structure). Solvent: DMSO:water (9:1).

Compound	τ_{F1} (ns)[a] (±2.7)	τ_{F2} (ns)[a] (±1.2)	τ_{F3} (ns)[a] (±0.2)
MPA QDs alone	19.0 (0.23)	4.8 (0.33)	0.9 (0.45)
ZnMAPPc + MPA QDs	14.1 (0.25)	3.8 (0.37)	0.8 (0.38)
TGA QDs alone	23.6 (0.28)	4.4 (0.27)	0.8 (0.45)
ZnMAPPc +TGA QDs	18.5 (0.19)	2.9 (0.24)	0.4 (0.57)
L-Cys alone	10.9 (0.03)	2.8 (0.21)	0.6 (0.76)
ZnMAPPc + L-Cys QDs	11.0 (0.03)	2.9 (0.21)	0.6 (0.76)

[a]Relative abundance in brackets.

It is important to know the number of emissive species for the interpretation of fluorescence results and time-resolved emission spectroscopy (TRES) is useful in this regard. In TRES, the fluorescence lifetime is automatically recorded as a function of emission wavelength. Figure 9 shows the TRES of zinc phthalocyanine (ZnMTPc), see Fig. 1c for structure [52]. The inset in Fig. 9 shows the emission spectra of the monomeric (Fig. 9, inset i) and aggregated (Fig. 9, inset ii) forms of the Pc, with the aggregated species of the Pc having shorter fluorescence lifetime, whereas the monomeric species

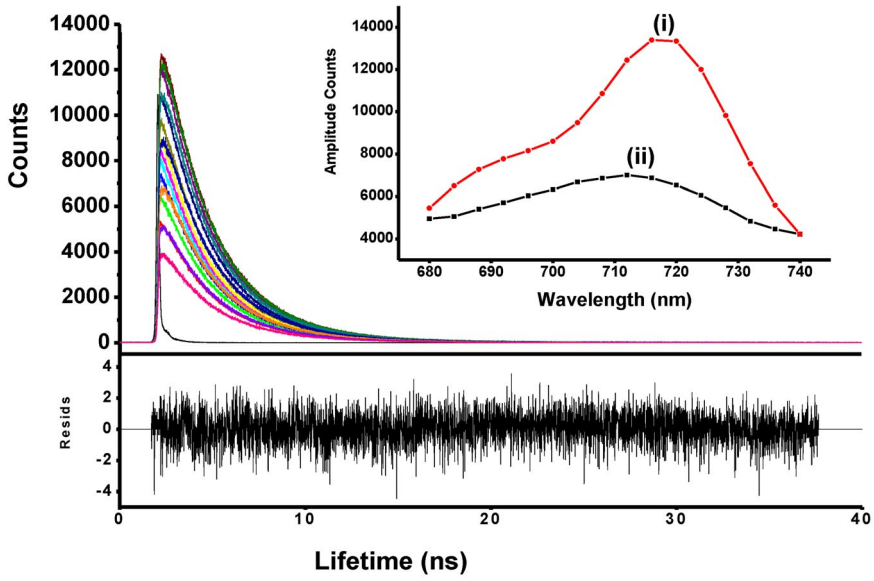

Fig. 9 TRES photoluminescence decay curves of ZnMTPc in DMSO ($\lambda_{excitation}$ = 722 nm, measurements taken at the maximum of the exciton emission peak, $\tau_{1/e}$ = 4.58 ns) adapted from ref. [52].

exhibits longer fluorescence lifetime. Thus, the monomeric species corresponds to the emission peak with higher intensity while the aggregated specie corresponds to the lower intensity peak in Fig. 9 (inset).

Förster resonance energy transfer

FRET is a nonradiative ET from a photoexcited donor fluorophore, to an acceptor fluorophore of a different species which is in close proximity. This ET is mainly dependent on: the center-to-center separation distance between donor and acceptor (r), the degree of spectral overlap of the donor's fluorescence emission spectrum and the acceptor's absorption spectrum (J), and the orientation of the donor and acceptor transition dipoles [53]. In order for FRET to occur, there should be an overlap between the fluorescence spectra of QDs (donor) with the absorption spectrum of acceptor (MPc), Fig. 10. The occurrence of FRET is evidenced by a decrease of the donor photoemission accompanied by an increase in the acceptor's fluorescence, Fig. 11. However, the acceptor may or may not be fluorescent for FRET to occur.

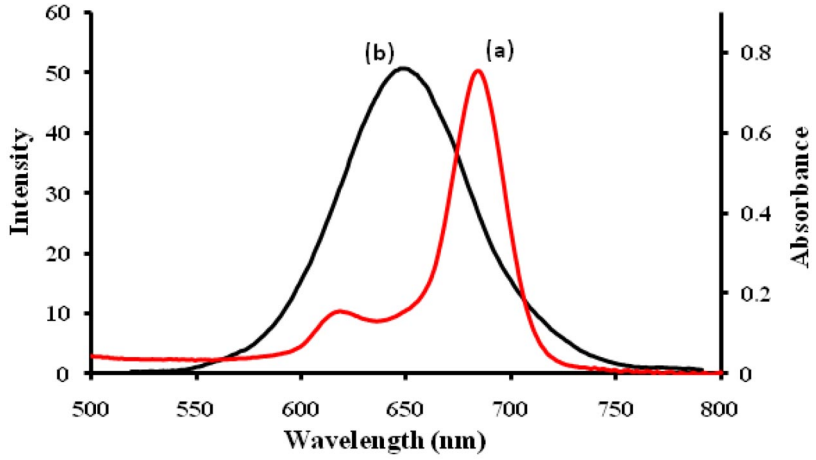

Fig. 10 Absorbance (a) of ZnMTPc (structure in Fig. 1c) and emission spectra (b) of MPA-capped CdTe QDs. (in (1:1) ethanol: 0.01 M NaOH solvent mixture, QDs $\lambda_{excitation}$ = 500 nm). Adapted from ref. [52].

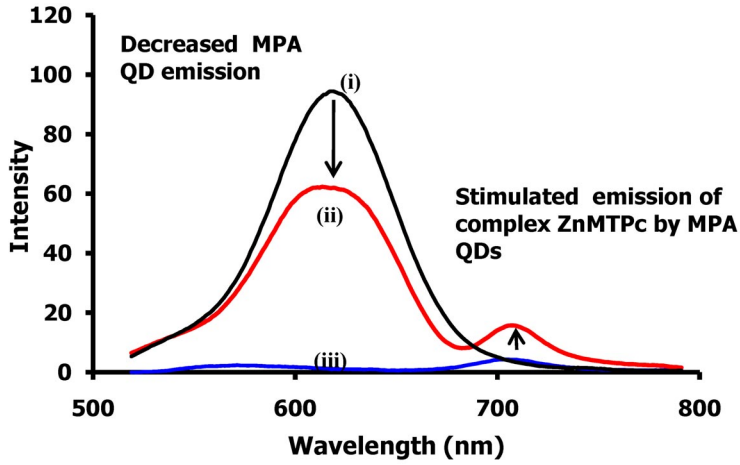

Fig. 11 Emission of MPA CdTe QDs in the absence (a) and presence (b) of MPc Fig. 1c. $\lambda_{excitation}$ = 500 nm, in (1:1) ethanol:0.01 M NaOH solvent mixture. Adapted from ref. [52].

The FRET efficiency (*Eff*) is determined experimentally from the fluorescence quantum yields of the donor in the absence ($\Phi_{F(QD)}$) and presence ($\Phi^{mix}_{F(QD)}$) of the acceptor using eq. 20 [53].

$$Eff = 1 - \frac{\Phi^{mix}_{F(QD)}}{\Phi_{F(QD)}} \tag{20}$$

The FRET efficiency may also be determined using average fluorescence lifetimes of the donor (e.g., MPA CdTe QDs) in the presence of (τ_{DA}) and the absence (τ_D) of the acceptor (a Pc complex) using eq. 21.

$$Eff = 1 - \frac{\tau_{DA}}{\tau_D} \tag{21}$$

The efficiency of ET (*Eff*) is related to r (Å) by eq. 22 [53].

$$Eff = \frac{R_0^6}{R_0^6 + r^6} \tag{22}$$

where R_0 (the Förster distance, Å) is the critical distance between the donor and acceptor fluorophores at which the efficiency of ET is 50 %. R_0 depends on the quantum yield of the donor, eq. 23 [53]:

$$R_0{}^6 = 8.8 \times 10^{23}\ \kappa^2\ n^{-4}\ \Phi_{F(QD)}\ J \tag{23}$$

where n is the refractive index of the medium; $\Phi_{F(QD)}$, the fluorescence quantum yield of the donor in the absence of the acceptor; J is the Förster overlap integral; and κ^2 is the transition dipole orientation factor. In this case, it is assumed that κ^2 is 2/3. This assumption is often made for donor–acceptor pairs in a liquid medium. FRET parameters may be computed using the program PhotochemCAD [54]. J, the Förster overlap integral, is defined by eq. 24

$$J = \int f_{QD}\ (\lambda)\ \varepsilon_{MPc}\ (\lambda)\ \lambda^4\ \partial\lambda \tag{24}$$

where f_{QD} is the normalized QD emission spectrum; and ε_{MPc}, the molar extinction coefficient of the MPc derivative. λ is the wavelength of the acceptor (the Q-band). It is well established that FRET only takes place when r values are within the range of 2–10 nm [54]. As an example, Table 4, shows that the r values can be fairly small, suggesting that the MPc complexes are in close proximity to the donor (QDs), and thus there should be an ease of nonradiative energy transfer (FRET) from the excited CdTe MPA QDs to MPc molecules.

Table 4 ET parameters for ZnMTPc-CdTe MPA QD interactions.

Conjugate	Solvent	$J/10^{14}$ cm^6	$R_0/10^{10}$ m	$r/10^{10}$m	*Eff*
ZnMTPc + MPA QDs	(DMSO)	7.1	37.7	39.9	0.42
ZnMTPc + MPA QDs	(DMF)	7.0	35.6	33.7	0.58
ZnMTPc + MPA QDs	(EtOH: 0.01 M NaOH (1:1))	3.4	33	37.4	0.32

The values for J are generally of the order 10^{-14} cm^6 for the overlap between CdTe QDs and MPc complexes, Table 4. The relatively high value of J is an indication of good spectral overlap of the emission spectrum of the donor and the absorption spectrum of the acceptor.

Perspectives

For selectivity, the synthesis of Pcs monosubstituted with functional groups such as NH_2 or COOH is essential in order to allow for coordination to molecules such as folic acid, which are known to be specific to cancer cells. Such studies have been done for only a very few porphyrin photosensitizers due to the difficulty of synthesizing monosubstituted Pcs. The best central metals for use in PDT include Zn, Si, Ge due to relatively high triplet yields and long lifetimes. However, dark toxicity of the Pcs containing metals such as Ge is of concern. QDs transfer energy to Pcs when the two are in close proximity and when excitation is carried out at the wavelength where QDs absorb. The fluorescence quantum yield of the QDs decrease in the presence of Pcs, depending on the spectral overlap between the absorption spectrum of the Pc and the emission spectrum of the QDs.

ACKNOWLEDGMENTS

This work was supported by the Department of Science and Technology (DST) and National Research Foundation (NRF), South Africa through DST/NRF South African Research Chairs Initiative for Professor of Medicinal Chemistry and Nanotechnology as well as Rhodes University.

REFERENCES

1. P. Gregory. In: *High-Technology Applications of Organic Colourants*, pp. 7–273, Plenum Press, New York (1991).
2. N. B. McKeown. In: *Phthalocyanine Materials: Synthesis, Structure and Function. Chemistry of Solid State Materials*, pp. 32–149, Cambridge University Press, New York (1998).
3. I. Okura. In: *Photosensitization of Porphyrins and Phthalocyanines*, pp. 151–213, Gordon and Breach, Amsteldijk, Netherlands (2001).
4. D. Dini, M. Hanack. In *Phthalocyanines: Properties and Materials. The Porphyrin Handbook*, Vol. 17, K. M. Kadish, K. M. Smith, R. Guilard (Eds.), Chap. 107, pp. 1–31, Academic Press, New York (2003).
5. E. Ben-Hur, W. S. Chan. In: *Photobiology of Phthalocyanines: Phthalocyanines in Photobiology and their Medical Applications*. *The Porphyrin Handbook*, Vol. 19, K. M. Kadish, K. M. Smith, R. Guilard (Eds.), Chap. 117, pp. 1–30, Academic Press, New York (2003).
6. P. Gregory. *J. Porphyrins Phthalocyanines* **3**, 468 (1999).
7. P. Gregory. *J. Porphyrins Phthalocyanines* **4**, 432 (2000).
8. N. Kobayashi, H. Konami. In: *Phthalocyanines: Properties and Application*, Vol. 4, C. C. Leznoff, A. B. P. Lever (Eds.), VCH, New York (1999).
9. T. Nyokong. In: *Functional Phthalocyanine Molecular Materials, Structure and Bonding*, Vol. 135, J. Jiang (Ed.), Springer, New York (2010).
10. P. Tau, T. Nyokong. *Dalton Trans*. 4482 (2006).
11. G. Mbambisa, P. Tau, E. Antunes, T. Nyokong. *Polyhedron* **26**, 5355 (2007).
12. G. Mbambisa, T. Nyokong. *Polyhedron* **27**, 2799 (2008).
13. T. Fukuda, K. Ono, S. Homma, N. Kobayashi. *Chem. Lett.* **32**, 736 (2003).
14. N. Kobayashi, H. Ogata, N. Nonaka, E. A. Luk'yanets. *Chem.—Eur. J.* **9**, 5123 (2003).
15. J. Obirai, T. Nyokong. *Electrochim. Acta* **49**, 1417 (2004).
16. N. Nombona, P. Tau, N. Sehlotho, T. Nyokong. *Electrochim. Acta* **53**, 3139 (2008).
17. P. Tau, T. Nyokong. *J. Electroanal. Chem.* **611**, 10 (2007).
18. F. Dumoulin, M. Durmuş, V. Ahsen, T. Nyokong. *Coord. Chem. Rev*. **254**, 2792 (2010).
19. J. Gravier, R. Schneider, C. Frochot, T. Bastogne, F. Schmitt, J. Didelon, F. Guillemin, M. Barberi-Heyob. *J. Med. Chem*. **51**, 3867 (2008).
20. S. Maree, T. Nyokong. *J. Porphyrins Phthalocyanines* **5**, 782 (2001).
21. R. Bonnett. In *Chemical Aspects of Photodynamic Therapy*, pp. 199–222, Gordon and Breach, Amsteldijk, Netherlands (2000).
22. N. Kuznetsova, N. Gretsova, E. Kalmykova, E. Makarova, S. Dashkevich, V. Negrimovskii, O. Kaliya, E. Lukyanets. *Russ. J. Gen. Chem.* **70**, 133 (2000).
23. T. Nyokong, E. Antunes. In: *The Handbook of Porphyrin Science*, Vol. 7, K. M. Kadish, K. M. Smith, R. Guilard (Eds.), Chap. 34, pp. 247–349, Academic Press, New York, World Scientific, Singapore (2010).
24. P. Kubát, J. Mosinger. *J. Photochem. Photobiol. A: Chem*. **96**, 93 (1996).
25. A. O. Ogunsipe, T. Nyokong. *J. Photochem. Photobiol. A: Chem.* **173**, 211 (2005).
26. W. Spiller, H. Kliesch, D. Wohrle, S. Hackbarth, B. Roder, G. Schnurpfeil. *J. Porphyrins Phthalocyanines* **2**, 145 (1998).

27. N. A. Kuznetsova, N. S. Gretsova, O. A. Yuzhakova, V. M. Negrimovskii, O. L. Kaliya, E. A. Luk'yanets. *Russ. J. Gen. Chem.* **71**, 36 (2001).
28. I. Seotsanyana-Mokhosi, T. Nyokong. *J. Porphyrins Phthalocyanines* **8**, 1214 (2004).
29. A. O. Ogunsipe, T. Nyokong. *J. Porphrins Phthalocyanines* **9**, 121 (2005).
30. N. Kuznetsova, N. Gretsova, E. Kalmykova, E. Makarova, S. Dashkevich, V. Negrimovskii, O. Kaliya, E. Lukyanets. *Russ. J. Gen. Chem*. **70**, 133 (2000).
31. T. Nyokong. *Coord. Chem. Rev*. **251**, 1707 (2007).
32. M. S. Patterson, S. J. Madsen, R. Wilson. *J. Photochem. Photobiol. B: Biol.* **5**, 69 (1990).
33. P. Juzenas, W. Chen, Y.-P. Sun, M. A. V. N. Coelho, R. Generalova, N. Generalova, I. L. Christensen. *Adv. Drug Delivery Rev.* **60**, 1600 (2008).
34. D. K. Chatterjee, L. S. Fong, Y. Zhang. *Adv. Drug. Delivery Rev.* **60**, 1627 (2008).
35. A. C. S. Samia, X. B. Chen, C. Burda. *J. Am. Chem. Soc.* **125**, 15736 (2003).
36. A. C. S. Samia, S. Dayal, C. Burda. *Photochem. Photobiol.* **82**, 617 (2006).
37. Y. N. Konan-Kouakou, R. Boch, R. Gurny, E. Allemann. *J. Controlled Release* **103**, 83 (2005).
38. R. Bakalova, H. Ohba, Z. Zhelev, M. Ishikawa, Y. Baba. *Nat. Biotechnol.* **22**, 1360 (2004).
39. C. Seydel. *Science* **300**, 80 (2003).
40. X. H. Gao, S. M. Nie. *J. Phys. Chem. B* **107**, 575 (2007).
41. N. Y. Morgan, S. English, W. Chen, V. Chernomordik, A. Russo, P. D. Smith, A. Gandjbakhche. *Acad. Radiol.* **12**, 313 (2005).
42. M. Idowu, T. Nyokong. *Polyhedron* **28**, 891 (2009).
43. S. Moeno, T. Nyokong. *J. Photochem. Photobiol. A: Chem.* **203**, 204 (2009).
44. J. Britton, E. Antunes, T. Nyokong. *J. Photochem. Photobiol. A: Chem*. **210**, 1 (2010).
45. S. Fery-Forgues, D. Lavabre. *J. Chem. Educ*. **76**, 1260 (1999).
46. D. V. Talapin, A. L. Rogach, E. V. Shevchenko, A. Kornowski, M. Haase, H. Weller. *J. Am. Chem. Soc*. **124**, 5782 (2002).
47. S. D'Souza, E. Antunes, T. Nyokong. *Inorg. Chim. Acta* **367**, 173 (2011).
48. X. Wang, L. Qu, J. Zhang, X. Peng, M. Xiao. *Nano Lett*. **3**, 1103 (2003).
49. M. Lunz, A. Louise Bradley. *J. Phys. Chem. C* **113**, 3084 (2009).
50. J. Zhang, X. Wang, M. Xiao. *Opt. Lett*. **27**, 1253 (2002).
51. M. G. Bawendi, P. J. Carroll, W. L. Wilson, L. E. Bruce. *J. Chem. Phys.* **96**, 946 (1992).
52. S. Moeno, E. Antunes, T. Nyokong. *J. Photochem. Photobiol. A: Chem.* **218**, 101 (2011).
53. J. R. Lakowiecz. *Principles of Fluorescence Spectroscopy*, 2nd ed., Kluwer Academic/Plenum Publishers, New York (1999).
54. H. Du, R. A. Fuh, J. Li, L. A. Corkan, J. S. Lindsey. *Photochem. Photobiol*. **68**, 141 (1998).

